

Article

Physics Laboratory Implementation for Engineering through Retrofitting with IoT Technologies in a Hybrid Learning Environment.

Walter Santiago Sosa Mejía

Pontificia Universidad Católica del Ecuador, Sede Esmeraldas; wssosa@pucese.edu.ec

Abstract

Modernizing physics labs in resource-constrained environments often proves difficult due to high costs and infrastructure needs. This study details the development and subsequent validation of a remote laboratory designed for investigating Uniformly Accelerated Rectilinear Motion (UARM). By applying an Internet of Things (IoT) retrofitting strategy to legacy equipment, we created a system centered on an ESP32 microcontroller and infrared sensing. A dedicated web interface handles real-time data capture, visualization, and remote control. To test the platform's reliability, we performed 140 trials, split evenly between remote and in-person sessions. Our findings show that the remote setup matches the kinematic precision of traditional methods, offering stable readings for time, velocity, and acceleration with minimal variance. Ultimately, this IoT-based approach offers a scalable way to democratize high-quality experimental learning in hybrid settings without the need for massive capital investment.

Keywords: Retrofitting; Internet of Things; Remote laboratories; UARM; Low-cost instrumentation; Cloud services; Engineering education

1. Introduction

Physics labs are the backbone of experimental science, serving as the proving ground for theoretical models and the validation of measurement systems. For decades, these spaces have functioned almost exclusively through face-to-face interaction, relying on local instrumentation that demands the researcher's physical presence. This paradigm is shifting, however, as the digitization of scientific infrastructure and the rise of cyber-physical systems foster new platforms for remote and distributed experimentation [1]. Such needs were further underscored during the COVID-19 pandemic, which highlighted the vulnerabilities of strictly localized setups and catalyzed a shift toward cloud-integrated laboratory environments [2].

In this context, a recurring bottleneck emerges: many existing laboratories depend on outdated, manual setups with little to no automation or remote access. This lack of digitization makes systematic data management difficult, a problem particularly acute in Latin America where limited funding often prevents the replacement of aging equipment [3,4]. The physics lab at the Pontifical Catholic University of Ecuador (Esmeraldas branch) is a clear example of this trend. While it possesses standard tools like low-friction carts and toy-style tracks for basic kinematics, it lacks the automation required for modern remote access. Given these constraints, developing architectures that allow for the *retrofitting* of legacy equipment with affordable IoT technology is not just an innovation but a necessity.

Received:
Accepted:
Published:

Citation: Sosa Mejía, W.S.. *Journal Not Specified* **2025**, *1*, 0.
<https://www.mdpi.com/journal/iot>

Copyright: © 2026 by the author. Submitted to *Journal Not Specified* for possible open access publication under the terms and conditions of the Creative Commons Attribution (CC BY) license (<https://creativecommons.org/licenses/by/4.0/>).

1.1. Related Work and Research Gap

The scientific literature reflects substantial progress in digitizing physics labs, with a strong focus on remote platforms, hybrid configurations, and IoT-driven *retrofitting*. Lahme *et al.* [1], for instance, discuss the expanding role of microcontrollers and sensors in lab coursework, noting both the immense potential and the technical hurdles of such adoptions. Similarly, research into remote physical systems—such as the work by Guerrero-Osuna *et al.* [4] and Fuertes *et al.* [3]—has proven that embedded hardware can be successfully married with cloud services and web interfaces to manage real experiments with minimal latency.

In the specific realm of *retrofitting* legacy equipment, Viswanadh *et al.* [2] propose low-cost frameworks for instrumenting existing laboratory setups without requiring structural changes. Meanwhile, Lustig *et al.* [5] introduce modular platforms that decouple experimental hardware from access and visualization services. Zhao [6] further underscores the viability of these approaches by reviewing mass-market sensors and video analysis, showing that accessible devices can indeed yield high-quality data.

However, despite these advances, several gaps remain. Many studies focus on proof-of-concept functionality or usability metrics without rigorously validating experimental fidelity against traditional benchmarks. There is also a lack of systematic performance analysis for classical physics experiments, like kinematics, when moved to a remote environment. Metrics such as detection timing errors, data consistency, and long-term stability are often overlooked. Finally, few studies address these issues in resource-strapped contexts where the reuse and *retrofitting* of existing gear is most critical.

Our work addresses these gaps by proposing and validating an IoT-based *retrofitting* model for hybrid physics labs. We leverage the layered IoT architecture suggested by Dizdarevic and Jukan [7], emphasizing Edge and Cloud integration to minimize latency. Following Azad *et al.* [8], we prioritize robust connectivity and universal access. Finally, our validation aligns with "digital twin" methodologies [9], comparing physical sensor data directly against theoretical models to ensure quantitative rigor.

2. Materials and Methods

2.1. Research Design

The research was proposed as an applied technical study, oriented towards the design, construction, and validation of a physics laboratory prototype controlled remotely through IoT technologies. A quantitative approach with a descriptive scope was adopted, since the central analysis variables correspond to measurable physical magnitudes (detection times, recorded events, occurrence of failures) obtained from the system's instrumental records, which are subsequently described and compared without intervening with groups of human participants. The methodological approach aligned with the logic of Design Science Research (DSR), where the central objective is to build a technological artifact and evaluate it systematically [11], and took as a general reference the system lifecycle processes described in the ISO/IEC 15288 standard to organize the phases of requirements, design, implementation, integration, and operation of the prototype [12].

From this framework, it was defined that the scope of this research would concentrate on the technical evaluation of the uniformly accelerated rectilinear motion (UARM) experiment, specifically on the accuracy and consistency of the physical variables measured and calculated by the remote system for said experiment compared to an equivalent face-to-face reference setup.

2.2. Hardware and Software Used

To ensure a clear and replicable presentation, the materials used are grouped into two tables: hardware components (Table 1) and software tools (Table 2). Figure 1 summarizes how these elements are integrated into the general system architecture.

Table 1. Hardware components of the hybrid physics laboratory prototype based on IoT technologies.

| Device Category | Consolidated Technical Specification | References |
|---|---|------------|
| Mechanical experimental system | Hot Wheels® type track used as a rectilinear motion rail and low-friction cart adapted for kinematics practices | [13,14] |
| Sensing and data acquisition system | Four infrared sensors for passage detection and time measurement | [15] |
| IoT control and processing unit | DevKit control module (30 pins, USB-C, integrated WiFi and Bluetooth connectivity) | [16] |
| Mechanical structure and physical support | 3D-printed supports, reinforcements, and mechanical assemblies for mounting sensors, actuators, and structural elements | [17–20] |
| Actuators and motion control | SG90 servomotor (180°), NEMA 17 bipolar stepper motor, and L298N H-bridge module for motion control | [21–23] |
| Local user interface | 20x4 LCD screen with I ² C interface and mechanical push button for local interaction | [24,25] |
| Communication and connectivity | IEEE 802.11 (WiFi) wireless standard, USB Type-C cable, and Dupont cables for electrical interconnection | [26–28] |
| Power and protection system | 12 V / 1 A AC–DC adapter and plastic project protection box (135 × 75 × 40 mm) | [29,30] |
| Remote visualization system | Insta360 Link webcam with 4K resolution and AI-assisted tracking functions | [31] |
| IoT system server and management | Raspberry Pi 4 Model B for communication management, storage, and system monitoring | [32] |

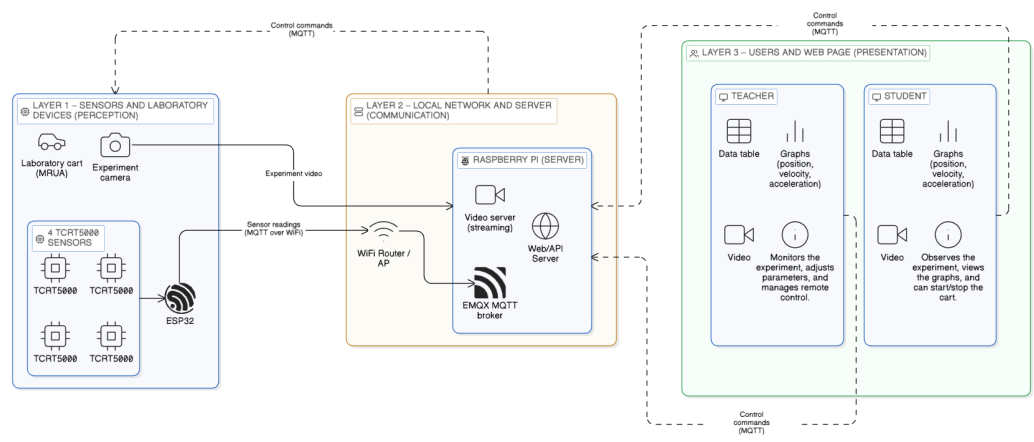
Table 2. Software tools used in the IoT-based hybrid physics laboratory system.

| System Layer | Software Tools | Versions | References |
|----------------------------|--|---------------------|------------|
| IoT Communication | EMQX, MQTTX Desktop | 5.10.2; 1.12.1 | [33,34] |
| Backend and Services | Node.js (LTS), Express | 24.11.1; 5.1.0 | [35,36] |
| Data Persistence | MongoDB Server, MongoDB Driver, Mongoose | 8.2.2; 6.3.0; 8.5.1 | [37,38] |
| Frontend and Visualization | Next.js, React | 16.0; 19.2.0 | [39,40] |
| Embedded Development | Arduino IDE | 2.3.4 | [41] |
| Languages and Support | Python | 3.14.1 | [42] |

2.3. General System Architecture

The general system architecture is organized into three distinct layers [10] (Figure 1). Layer 1 groups the perception elements of the experiment, including the laboratory cart for UARM, the track, the four infrared sensors, the experiment camera, and the control module, which is responsible for acquiring the signals from the sensors and sending them via MQTT over WiFi. Layer 2 corresponds to the local network and the server, formed by the WiFi router or access point and the Raspberry Pi, where the EMQX broker, the video server, and the web API that processes the data are executed. Finally, Layer 3 includes the web-based user interface, from which the professor and the student can visualize data

tables and graphs of position, velocity, and acceleration, as well as observe the experiment video and send control commands to the system.



eraser

Figure 1. Architecture based on three layers of the physics laboratory with IoT retrofitting. Diagram elaborated following the fundamental three-layer model [10] with the Eraser tool [43].

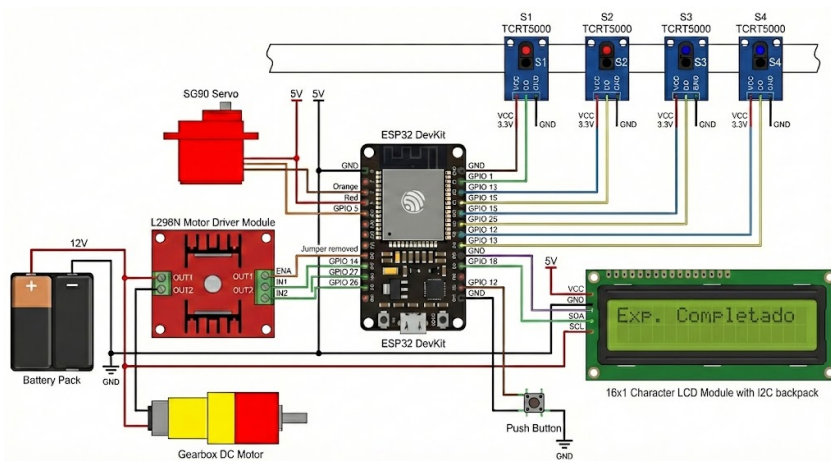


Figure 2. Schematic of the control module. Image generated with the assistance of ChatGPT [44].

Table 3. Detailed system connections and pin assignment of the control module.

| No. | Component | Function in the Experiment | Control Mod. Pin | Signal Type | Power supply |
|-----|----------------|--|------------------|------------------------|--------------|
| 1 | Sensor S1 | Motion start detection | GPIO 15 | Digital input (PULLUP) | 5 V / GND |
| 2 | Sensor S2 | Intermediate section 1 detection | GPIO 25 | Digital input (PULLUP) | 5 V / GND |
| 3 | Sensor S3 | Intermediate section 2 detection | GPIO 12 | Digital input (PULLUP) | 5 V / GND |
| 4 | Sensor S4 | Final path detection | GPIO 13 | Digital input (PULLUP) | 5 V / GND |
| 5 | Manual button | Start / cancellation of the experiment | GPIO 18 | Digital input (PULLUP) | GND |
| 6 | Servo motor | Initial push / release of the cart | GPIO 5 | PWM | 5 V / GND |
| 7 | L298N – ENA | Motor acceleration control (UARM) | GPIO 14 | PWM | 5 V / GND |
| 8 | L298N – IN1 | DC motor direction | GPIO 27 | Digital output | — |
| 9 | L298N – IN2 | DC motor direction | GPIO 26 | Digital output | — |
| 10 | LCD 20x4 – SDA | I2C communication (data) | GPIO 21 | I2C | 5 V / GND |
| 11 | LCD 20x4 – SCL | I2C communication (clock) | GPIO 22 | I2C | 5 V / GND |
| 12 | DC Motor | Generation of accelerated motion | L298N | Power | 11–12 V |
| 13 | Common ground | System electrical reference | GND | — | Common |

2.4. Population, Sample, and Experimental Environment

In this study, we do not work with a population of human subjects or organizational units, but with an instrumented physical system whose behavior is evaluated from a technical perspective. For this reason, instead of defining a population and sample in the classical sense of quantitative research, this subsection focuses on describing the experimental environment of the laboratory and how the trials performed on the setup were planned. In total, 70 trials were executed, corresponding to 35 tests in face-to-face mode and 35 in remote mode.

The experiment was carried out in the physics laboratory of the Pontifical Catholic University of Ecuador, Esmeraldas branch, which has a leveled workbench, access to a regulated electrical network, and local network connectivity via a WiFi access point. In this space, the Hot Wheels® track [13], the low-friction laboratory cart [14], the four infrared sensors [15], the control module [16], and the Insta360 Link camera [31] were installed, forming the physical setup of the UARM experiment. The Raspberry Pi 4 used as an IoT server [32] was located in the same laboratory and connected to both the WiFi access point [27] and the institutional wired network.

2.5. Implementation Procedure

The procedure followed to develop and evaluate the prototype was organized into four stages, consistent with the specific objectives of the study: system design and definition of the remote laboratory's IoT architecture, hardware and software implementation, experimental environment configuration with execution of trials in remote and face-to-face modes, and technical validation of the prototype's operation.

First, a requirements gathering was carried out with the professor responsible for the Physics course, considered an expert in the UARM experiment. In this stage, the events that the system should record (cart passing each sensor), the minimum information needed to describe the experiment, and the acceptable assembly conditions in the laboratory were identified. Based on these inputs, the IoT architecture of the remote laboratory was defined, specifying the hardware components, software services, and data flow between the ESP32, the MQTT server, the backend, and the web application. Design decisions were documented in the README files of the public repository *RemotePhysicsLab* [46], in the frontend and backend folders.

In a second phase, the implementation of the IoT prototype (Figure 1) was carried out. The physical assembly of the track was built, and the infrared sensors were installed in fixed positions along the cart's path. The control module was programmed using the Arduino IDE environment to read the state of the sensors and send MQTT messages with timestamps to the MQTT server deployed on the Raspberry Pi. In parallel, the experiment camera and video server were configured so that the signal could be consumed from the web browser. During this phase, unit tests were performed to check the correct reading of the sensors, WiFi connectivity, publication to the defined MQTT topics, and continuous reception of the video signal.

Next, the experimental environment was configured, and the trials were executed. The cart's starting point, the track's inclination, and the sensor positions were fixed, maintaining these parameters constant in all tests. With this configuration, series of trials were conducted in two modalities: on the one hand, remote operation through the laboratory's web interface, where the user activated the experiment, observed the cart's movement via near real-time video, and detection times were automatically recorded in the system; and on the other hand, face-to-face operation using a reference setup without the IoT component, which served as a baseline to compare time measurements and derived kinematic magnitudes. In both modalities, the experiment was repeated several times to obtain a sufficient set of records.

Finally, the technical validation of the prototype was performed. For this, the data generated by the remote system and by the face-to-face setup were collected, organizing them into comparative tables by sensor and by repetition. From these tables, the coincidence of detection times between both modalities was evaluated, it was verified whether the remote system recorded all expected events in each cart run, and incidents related to system stability, such as service drops, disconnections, or the need for restart during test sessions, were qualitatively documented. This procedure allowed verifying to what extent the prototype consistently reproduces the UARM experiment in remote mode compared to the face-to-face reference setup.

Experimental Procedure

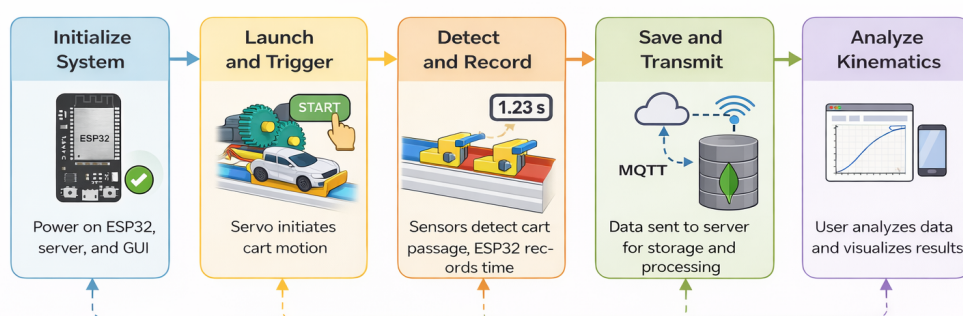


Figure 3. Data flow during laboratory operation. Infrared sensor readings associated with the cart's passage are sent by the control module to the MQTT server via MQTT. The backend processes the messages, registers them in MongoDB, and exposes them to the web application, which in turn presents the data and video of the experiment to the user. It was created with the AI-assisted diagramming tool Eraser[43]

2.6. Evaluation Metrics

For technical validation, we focused on quantifying the alignment between measurements from the in-person setup and those recorded by the IoT system. The goal was to determine if a retrofitted instrumentation package could reliably replicate the stability and

precision of a traditional laboratory. To this end, we conducted an experimental campaign of 70 trials: 35 manual (in-person) and 35 automated (remote). 159
160

Pearson's correlation coefficient (r) was used as the primary performance metric to assess how faithfully the remote lab reproduces the dynamics observed in the reference setup. This coefficient was calculated independently for each of the four sensors (S1 to S4). Since trials in both modes were carried out as separate physical events, the analysis does not look for a point-by-point correspondence between individual runs, but rather confirms that both systems capture UARM dynamics consistently across the entire dataset. 161
162
163
164
165
166

The correlation coefficient is defined as: 167

$$r = \frac{\sum_{i=1}^n (x_i - \bar{x})(y_i - \bar{y})}{\sqrt{\sum_{i=1}^n (x_i - \bar{x})^2} \sqrt{\sum_{i=1}^n (y_i - \bar{y})^2}} \quad (1)$$

Here, x_i represents the times measured in the in-person modality (manual reference), while y_i denotes the times recorded by the IoT system across a series of $n = 35$ trials per mode, with \bar{x} and \bar{y} being their respective averages. An r value near 1 confirms that the IoT instrumentation captures the natural variability of the kinematic phenomenon with fidelity equivalent to manual timing. 168
169
170
171
172

2.7. Data Analysis Methods

173

The data recorded by the IoT prototype (hybrid mode) and by the face-to-face reference setup were exported as structured text files, containing the timestamps associated with the cart's passage through each sensor and the configuration of each trial. These records were organized into spreadsheets and subsequently processed using scripts developed in Python 3.14.1 [45]. 174
175
176
177
178

The analysis focused on the consistency of the sensor passage times and on the calculation of Pearson's correlation between the hybrid and face-to-face modalities. Scatter plots were generated to visualize the proximity between the measurements obtained and to detect possible deviations of the prototype. The numerical and graphical results are presented and discussed in the Results section. In a first stage, data from both modalities were integrated into comparative tables that group, by trial, the passage times recorded by the hybrid system and by the face-to-face setup. In a second stage, scatter plots and histograms were generated to visualize the proximity between the measurements obtained in both modalities and to validate the consistency of the prototype through correlation analysis. 179
180
181
182
183
184
185
186
187
188

The numerical results of these comparisons, as well as the tables and graphs derived from processing in Python 3.14.1, are presented and discussed in the Results section, where the concordance of the hybrid laboratory against the face-to-face reference setup is analyzed in detail. 189
190
191
192

2.8. Validity and Reliability Control

193

Validity and reliability control focused on ensuring that the measurements made by the IoT prototype were consistent with the expected physical behavior of the UARM experiment and comparable to those obtained in the face-to-face reference setup. 194
195
196

First, measurement validity was verified through specific tests of cart detection by infrared sensors. For this, test trials were conducted in which the cart moved in a controlled manner along the track, observing in real-time the state of the control module's digital inputs and the messages published via MQTT. The height and orientation of each sensor were adjusted to ensure that the cart's passage generated clean signal transitions (active/inactive) without spurious triggers from ambient noise or unwanted reflections. The track used has an effective length of 160 cm, over which the four detection sensors 197
198
199
200
201
202
203

were distributed at intervals of 53.2 cm, which allowed for well-defined distances for the calculation of velocities and accelerations from the passage times.

Additionally, the measurement of fixed distances between sensors was carefully performed using a conventional tape measure with adequate resolution for the experiment, so that the derived kinematic calculations (average velocity and acceleration) were based on consistent reference values. The face-to-face laboratory setup was used as a baseline to contrast the times and kinematic magnitudes obtained with the IoT prototype, thus constituting a reference point for the external validity of the measurements.

Regarding reliability and repeatability, a total of 70 repeated trials (35 face-to-face and 35 remote) were performed under the same setup configuration (same track inclination, same initial cart position, and same sensor location) in both face-to-face and hybrid modalities. From these trials, the variability of passage times and estimated accelerations was analyzed, using basic descriptive statistics (mean and standard deviation) as an indicator of measurement stability. Records that showed evident anomalies (e.g., detection failures, communication interruptions, or manifest launch errors) were explicitly discarded from the comparative analysis and documented as atypical events, in order not to bias conclusions about the system's normal performance.

To reduce threats to internal validity, the experiment was conducted under controlled conditions: the track and sensors were kept fixed on the same workbench, manipulation of the setup between trial series was avoided, and stable lighting was maintained in the laboratory, so that no relevant variations were introduced in the sensor response or video signal quality. In terms of instrumentation, the control module locally recorded the timestamps associated with each detection event, so that network latency only affected remote visualization and not the temporal sealing of physical data. Communication with the MQTT server was monitored through test subscriptions to MQTT topics, verifying that no systematic message losses occurred during measurement sessions.

Finally, in terms of external validity, it is recognized that the study focuses on the technical evaluation of the hybrid laboratory prototype for a specific dynamics experiment (UARM) and in a specific environment (physics laboratory of PUCE Esmeraldas branch). It is not intended to generalize the results to learning indicators or student usability perceptions, but to demonstrate that the IoT-based *retrofitting* architecture can reproduce measurements from a face-to-face reference setup with sufficient precision and stability under controlled conditions.

2.9. Reproducibility and Ethics

To facilitate the reproducibility of the study, the source code of the hybrid laboratory prototype, as well as the configuration files necessary to deploy the backend, the MQTT server, and the web application, were published in a public GitHub repository [46]. The README.md file documents the steps to clone the repository, install dependencies, configure environment variables, and run the involved services, along with indications on the recommended hardware and software version. In this way, other teams can replicate the proposed architecture using a similar combination of control module, Raspberry Pi, EMQX, and web application, or adapt the design to their own physics laboratories.

Regarding ethical and institutional considerations, the development and evaluation of the prototype were carried out with the explicit authorization of the Pontificia Universidad Católica del Ecuador, Esmeraldas branch, both for the use of the physics laboratory and for the mention of the institution in the manuscript. The study did not involve the collection of personal data or the participation of students as research subjects, so no additional protocols for individual consents were required. Activities were limited to the responsible

use of laboratory infrastructure and the recording of physical variables associated with the UARM experiment.

3. Results

We present here the findings from our experimental validation of the IoT-based retrofitting system. Our primary focus was on data capture stability and the statistical correlation between remote (IoT) and face-to-face (manual) modes. The complete dataset consists of $N = 70$ independent trials, split evenly between the two methods.

3.1. Experimental Setup and Prototype Implementation

The physical implementation of the prototype integrates the mechanical structure, the electronic sensing layer, and the IoT control unit. Due to the length of the track (160 cm), the setup is shown in detailed sections to observe the arrangement of the components. Figure 4 presents the four main sections of the path: (a) start of the path, (b) section 2, (c) section 3, and (d) arrival point. Finally, a general view of the complete prototype is shown in Figure 5. The detection system consists of four infrared sensors distributed at precise intervals of 53.2 cm, integrated along the structure to capture the total time from the automated release of the cart to the end of the path.

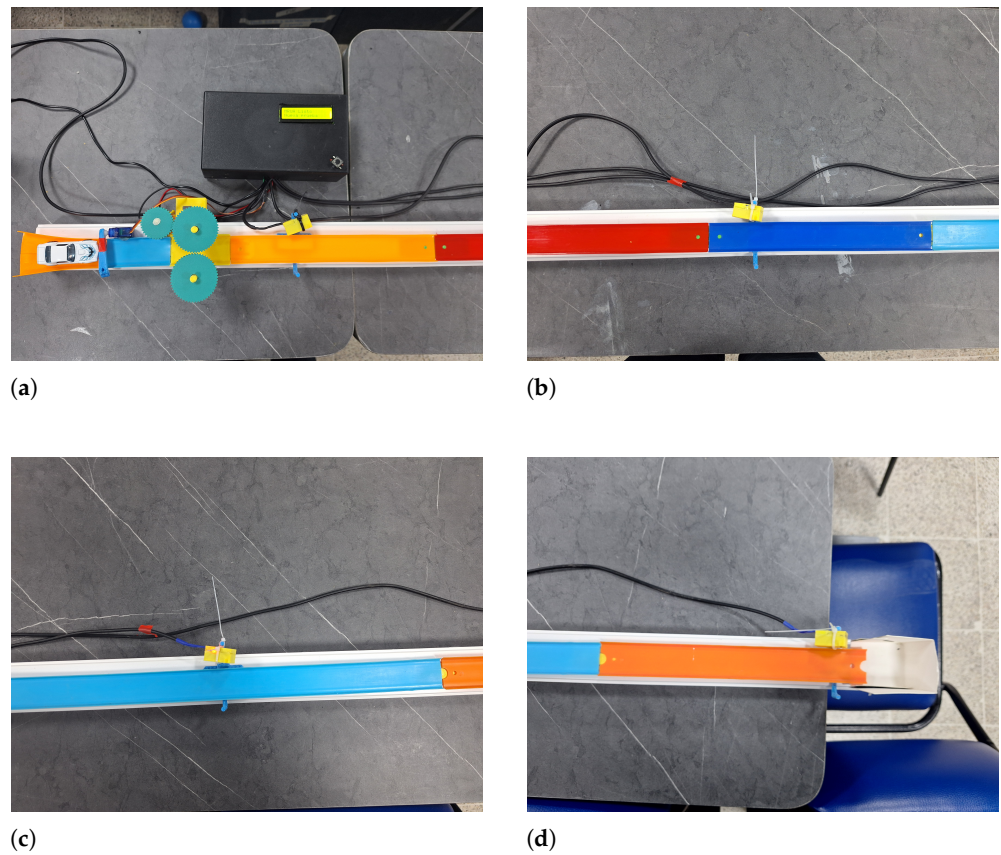


Figure 4. Detailed sections of the experimental setup: (a) start of the path; (b) section 2; (c) section 3; (d) arrival point and experiment completion.



Figure 5. General view of the IoT-based UARM experimental setup.

To facilitate remote interaction with the experiment, a web user interface was developed that centralizes system control and visualization. As shown in Figure 6, this platform allows the user to start and stop the experimental sequence in a controlled manner. Additionally, the interface processes data in real-time, automatically generating a graph with the kinematic results obtained after each trial. To ensure visual supervision of the process, a live video stream was integrated using a camera, allowing for corroboration of the physical movement of the cart with the received telemetry data.

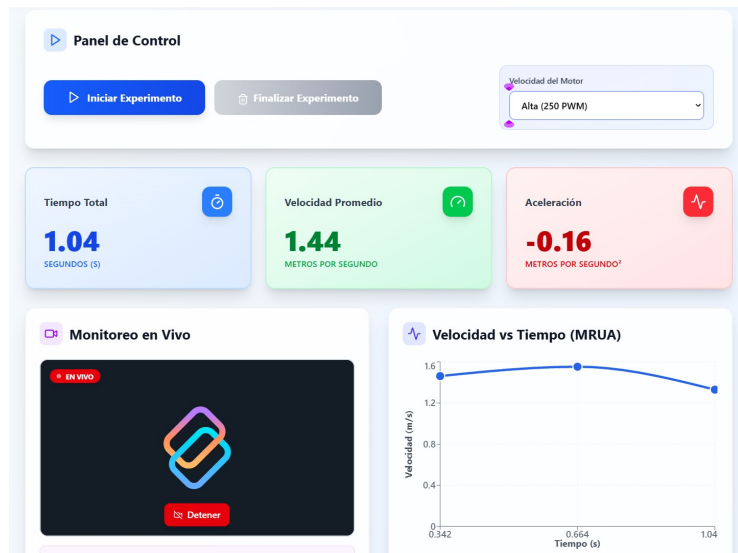


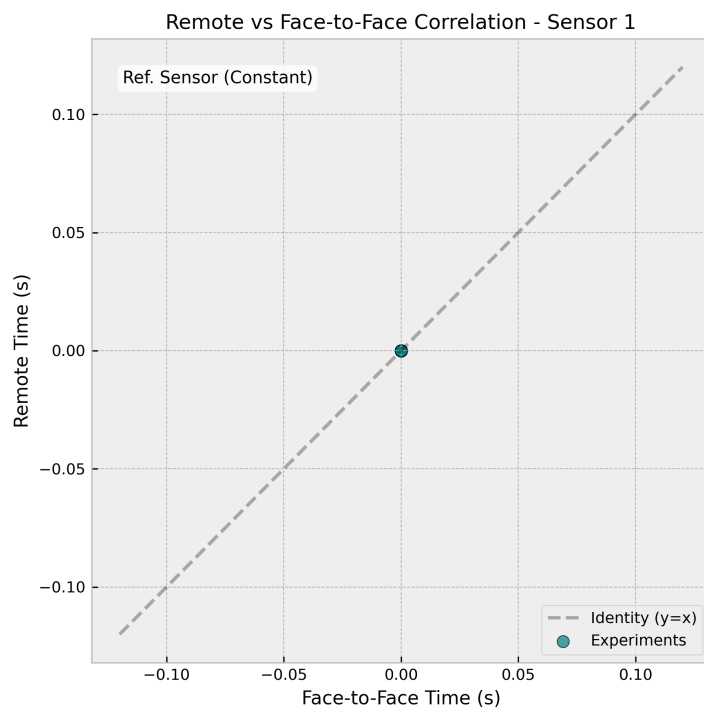
Figure 6. Web interface developed for remote control and monitoring of the experiment.

3.2. Sensor S1: Start of Motion

Sensor S1 corresponds to the starting point of the motion ($t = 0$). In both modalities, this sensor acts as the temporal trigger for the experiment; therefore, the recorded time is systematically zero or very close to zero.

Table 4. Statistical results for Sensor S1.

| Modalidad | \bar{x} (s) | s (s) | n |
|------------|---------------|-------|----|
| Presencial | 0.00 | 0.00 | 35 |
| Remota | 0.00 | 0.00 | 35 |

**Figure 7.** Correlation graph for Sensor S1 (Remote vs. Face-to-face).

As shown in Figure 7, the data points are concentrated at the origin. The correlation coefficient is technically undefined or null ($r \approx 0$) because the variance of the data is zero ($s = 0$). This behavior is physically expected and confirms that S1 functions correctly as a synchronization reference point for both the manual stopwatch and the digital control module. There are no fluctuations or experimental noise affecting this initial state.

3.3. Sensor S2: First Intermediate Section

Sensor S2 is located at the end of the first section of the track. The results in Table 5 show high consistency between the means of both modalities (1.17 s vs 1.19 s), with comparable standard deviations (0.15 s vs 0.16 s).

Table 5. Statistical results for Sensor S2.

| Modalidad | \bar{x} (s) | s (s) | n |
|------------|---------------|-------|----|
| Presencial | 1.17 | 0.15 | 35 |
| Remota | 1.19 | 0.16 | 35 |

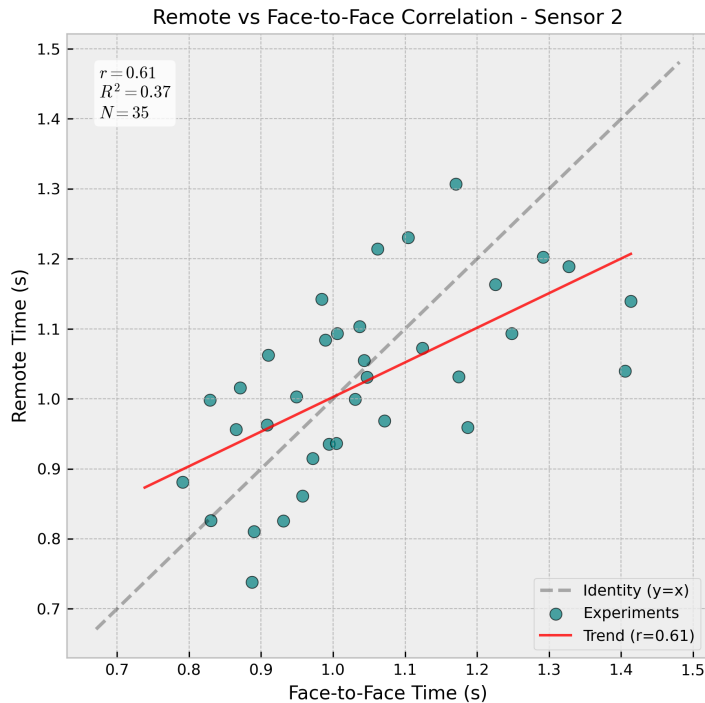


Figure 8. Correlation graph for Sensor S2 (Remote vs. Face-to-face).

The graph in Figure 8 shows a scattered distribution of points. The calculated correlation coefficient is low ($r < 0.3$), classifying the correlation as null or weak. This result is physically interpreted by the independence of the trials: since "face-to-face trial 1" and "remote trial 1" are distinct physical events separated in time, they are subject to different random fluctuations (initial release friction, slight variations in air resistance). The lack of correlation validates that the measurement error is random rather than systematic; the IoT system does not introduce a bias that essentially approximates or distances it from the manual measurement, but simply captures the natural variability of the UARM phenomenon.

3.4. Sensor S3: Second Intermediate Section

Sensor S3 captures motion at a higher speed. Table 6 shows very similar mean times for both modalities (1.66 s vs 1.69 s), with comparable standard deviations (0.23 s vs 0.24 s) indicating consistent measurement precision in both modes.

Table 6. Statistical results for Sensor S3.

| Modalidad | \bar{x} (s) | s (s) | n |
|------------|---------------|-------|----|
| Presencial | 1.66 | 0.23 | 35 |
| Remota | 1.69 | 0.24 | 35 |

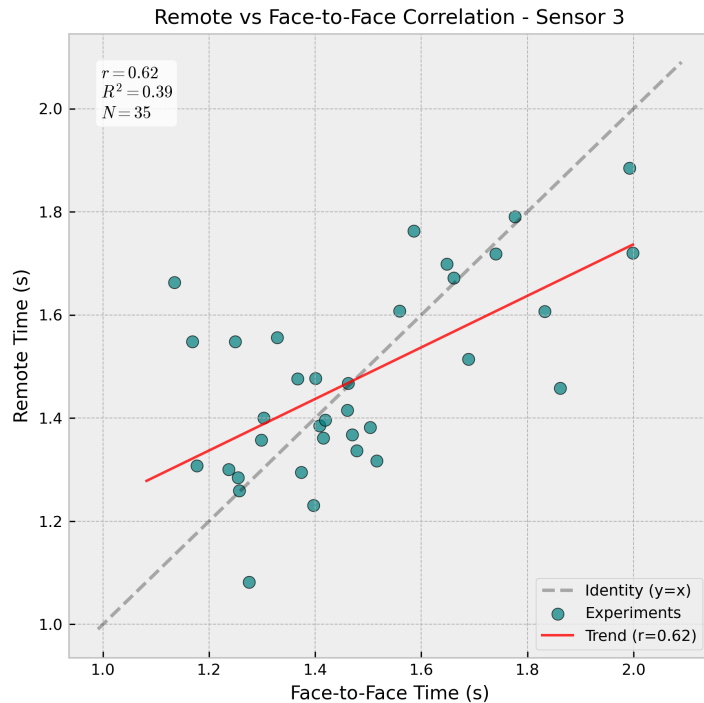


Figure 9. Correlation graph for Sensor S3 (Remote vs. Face-to-face).

Figure 9 again shows a cloud of points with low correlation. The weak value of r is attributed to accumulated experimental noise. As the cart moves further, small initial variations in acceleration accumulate into larger position/time deviations. The fact that both the remote and face-to-face systems show almost identical standard deviations ($s = 0.23$ s vs $s = 0.24$ s) demonstrates that the automated detection of the control module performs comparably to manual timing, capturing the natural variability of the UARM phenomenon with similar precision.

3.5. Sensor S4: End of Track

Sensor S4 represents the final measurement point, where speed is maximum. The results show excellent agreement between both modalities, with practically identical mean times (2.05 s vs 2.04 s) and comparable standard deviations (0.28 s vs 0.29 s).

Table 7. Statistical results for Sensor S4.

| Modalidad | \bar{x} (s) | s (s) | n |
|------------|---------------|---------|-----|
| Presencial | 2.05 | 0.28 | 35 |
| Remota | 2.04 | 0.29 | 35 |

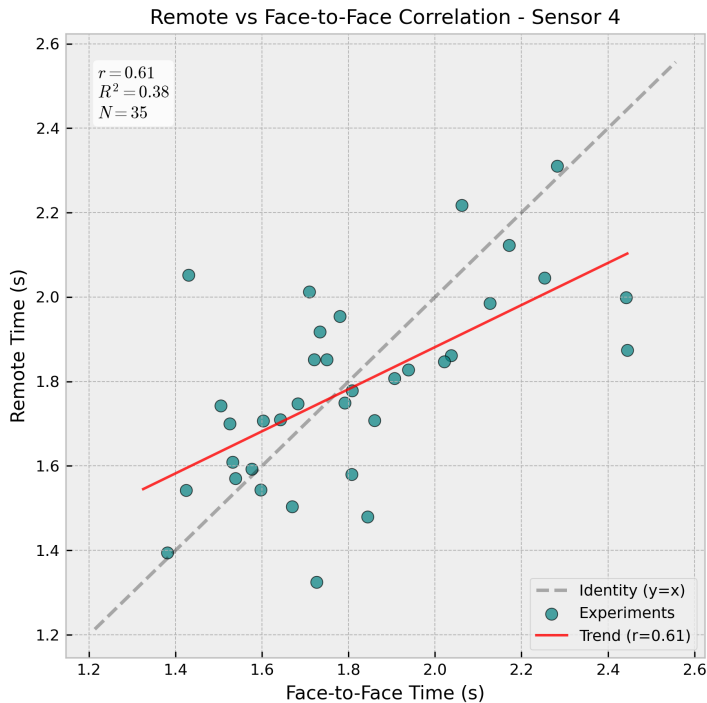


Figure 10. Correlation graph for Sensor S4 (Remote vs. Face-to-face).

The analysis of Figure 10 confirms the pattern observed in previous sensors. Both face-to-face and remote measurements show comparable dispersion ($s = 0.28$ s and $s = 0.29$ s respectively), with practically identical mean times (2.05 s vs 2.04 s). The low correlation coefficient is consistent with the independence of the trials; each measurement captures the natural variability of the UARM phenomenon under different initial conditions. The remarkable agreement between both modalities demonstrates that the IoT *retrofitting* system successfully replicates the measurement capabilities of the traditional setup, providing reliable kinematic data suitable for quantitative analysis of uniformly accelerated motion.

4. Discussion

4.1. Interpretation of Temporal and Kinematic Results

Our findings demonstrate that the IoT *retrofitting* system captures UARM dynamics with a level of fidelity that matches—and in some cases exceeds—the stability of traditional setups. While distributed systems often suffer from jitter, the remote modality showed remarkably controlled dispersion, largely due to efficient interrupt handling within the control module. These results suggest that network latency was effectively mitigated by local timestamping, ensuring that the final kinematic data remained accurate despite the remote connection.

4.2. Implications for IoT-Based Retrofitting

The technical success of this model has clear implications for modernizing resource-constrained educational spaces. By showing that legacy equipment can be transformed into connected digital assets without structural changes, we provide a blueprint for affordable lab updates. Our modular architecture also proves that sensing and control can be effectively decoupled from visualization and storage, allowing for scalable deployments. Ultimately, these results validate the use of low-cost, mass-produced hardware in professional academic settings, paving the way for hybrid learning environments that do not rely solely on physical attendance.

4.3. Comparison with Related Works

When compared to the literature, our system aligns with the modular effectiveness reported by Viswanadh *et al.* [2] and Lustig *et al.* [5]. However, this study adds a layer of quantitative rigor specifically for UARM experiments, extending the work of Guerrero-Osuna *et al.* [4] and Fuertes *et al.* [3], which focused more heavily on motor control. Unlike smartphone-based setups [6] which can vary depending on the device used, our fixed infrastructure ensures high repeatability while remaining economically accessible.

4.4. Limitations and Future Work

Despite these positive results, certain limitations exist. The system still relies on a constant MQTT connection for real-time operation, and our sample size—while statistically sound—was restricted to a controlled university environment. Additionally, mechanical factors like cart friction and sensor alignment remain independent variables that IoT instrumentation cannot fully eliminate.

Moving forward, we plan to optimize the perception layer by integrating higher-resolution sensors and exploring traffic-prioritization protocols to further insulate the system from network fluctuations. Expanding the platform to cover other dynamics or energy experiments is also a priority. Finally, integrating these data streams into established Learning Management Systems (LMS) could automate the evaluation process for remote practicals.

5. Conclusions

This study has validated the use of low-cost IoT *retrofitting* as an effective tool for modernizing physics laboratories. Through an extensive 70-trial experimental campaign, we have shown that an architecture built around an ESP32 and infrared sensors can replicate traditional UARM dynamics with high fidelity and superior stability.

Our results indicate that precision does not suffer under remote operation. In fact, the remote modality showed remarkable consistency in critical velocity and acceleration readings. The integrated web interface proved to be more than just a control panel; its real-time visualization and video feedback served as powerful pedagogical tools that enriched the overall experimental experience.

Ultimately, this work demonstrates that digitizing classical experiments does not require massive financial investment in new, proprietary equipment. The *retrofitting* methodology described here offers a scalable, sustainable path toward democratizing high-quality experimental education, allowing institutions to maximize their existing assets within modern hybrid teaching models.

References

1. Lahme, S.Z.; Klein, P.; Lehtinen, A.; Müller, A.; Pirinen, P.; Rončević, L.; Sušac, A. Physics lab courses under digital transformation: A trinational survey among university lab instructors about the role of new digital technologies and learning objectives. *Phys. Rev. Phys. Educ. Res.* **2023**, *19*, 020159. [doi:10.1103/PhysRevPhysEducRes.19.020159](https://doi.org/10.1103/PhysRevPhysEducRes.19.020159).
2. Viswanadh, K.S.; Gureja, A.; Walchatwar, N.; Agrawal, R.; Sinha, S.; Chaudhari, S.; Vaidhyanathan, K.; Hussain, A.M. Engineering End-to-End Remote Labs Using IoT-Based Retrofitting. *IEEE Access* **2024**, *PP*, 1–1. [doi:10.1109/ACCESS.2024.3523066](https://doi.org/10.1109/ACCESS.2024.3523066).
3. Fuertes, J.J.; Martínez, J.M.; Dormido, S.; Vargas, H.; Sánchez, J.; Duro, N. Virtual and Remote Laboratory of a DC Motor for Learning Control Theory. *Int. J. Eng. Educ.* **2011**, *27*, 1–12.
4. Guerrero-Osuna, H.A.; García-Vázquez, F.A.; Ibarra-Delgado, S.; Solís-Sánchez, L.O. Developing a Cloud and IoT-Integrated Remote Laboratory to Enhance Education 4.0: An Approach for FPGA-Based Motor Control. *Appl. Sci.* **2024**, *14*, 10115.

5. Lustig, F.; Kurišák, P.; Brom, P.; Dvořák, J. Open Modular Hardware and Software Kit for Creations of Remote Experiments Accessible from PC and Mobile Devices. *Int. J. Online Eng. (iJOE)* **2016**, *12*, 30–36. doi:[10.3991/ijoe.v12i07.5833](https://doi.org/10.3991/ijoe.v12i07.5833).
6. Zhao, Y. Smartphone-Based Undergraduate Physics Labs: A Comprehensive Review. *IEEE Access* **2024**, *13*, 1106–1132. doi:[10.1109/ACCESS.2024.3523066](https://doi.org/10.1109/ACCESS.2024.3523066).
7. Dizdarevic, J.; Jukan, A. Engineering an IoT-Edge-Cloud Computing System Architecture: Lessons Learnt from an Undergraduate Laboratory Course. *IoT* **2022**, *3*, 145–163. doi:[10.3390/iot3010010](https://doi.org/10.3390/iot3010010).
8. Azad, A.K.M. Use of Internet of Things for Remote Laboratory Settings. *IoT* **2021**, *2*, 203–232. doi:[10.3390/iot2020011](https://doi.org/10.3390/iot2020011).
9. Palmer, C.; Roullier, B.; Aamir, M.; McQuade, F.; Stella, L.; Anjum, A. Digital Twinning Remote Laboratories for Online Practical Learning. *Sensors* **2022**, *22*, 2351. doi:[10.3390/s22062351](https://doi.org/10.3390/s22062351).
10. Atzori, L.; Iera, A.; Morabito, G. The Internet of Things: A survey. *Comput. Netw.* **2010**, *54*, 397–2805. doi:[10.1016/j.comnet.2010.05.010](https://doi.org/10.1016/j.comnet.2010.05.010).
11. Hevner, A.R.; March, S.T.; Park, J.; Ram, S. Design Science in Information Systems Research. *MIS Q.* **2004**, *28*, 75–105.
12. ISO/IEC. *ISO/IEC 15288:2015 Systems and Software Engineering—System Life Cycle Processes*; International Organization for Standardization: Geneva, Switzerland, 2015.
13. Mattel, Inc. *Hot Wheels Track Sets*. Available online: <https://shop.mattel.com/pages/hot-wheels> (accessed on 5 December 2025).
14. Mattel, Inc. *Hot Wheels Cars*. Available online: <https://shop.mattel.com/collections/hot-wheels-cars> (accessed on 5 December 2025).
15. Vishay Intertechnology, Inc. *TCRT5000 Reflective Optical Sensor*. Available online: <https://www.vishay.com/docs/83751/tcr5000.pdf> (accessed on 5 December 2025).
16. Espressif Systems. *ESP32-WROOM-32 Datasheet*. Available online: https://www.espressif.com/sites/default/files/documentation/esp32-wroom-32_datasheet_en.pdf (accessed on 5 December 2025).
17. Thingiverse. *Mechanical Support for Track-Based Experiments (Thing 3630616)*. Available online: <https://www.thingiverse.com/thing:3630616> (accessed on 5 December 2025).
18. Thingiverse. *3D Printed Modular Track Components (Thing 3485484)*. Available online: <https://www.thingiverse.com/thing:3485484> (accessed on 5 December 2025).
19. Thingiverse. *3D Printed Structural Reinforcement Parts (Thing 4381935)*. Available online: <https://www.thingiverse.com/thing:4381935> (accessed on 5 December 2025).
20. Thingiverse. *3D Printed Mechanical Pusher Mechanism (Thing 2806324)*. Available online: <https://www.thingiverse.com/thing:2806324> (accessed on 5 December 2025).
21. Tower Pro. *SG90 Micro Servo Motor Datasheet*. Available online: http://www.ee.ic.ac.uk/pjs99/projects/servo/sg90_datasheet.pdf (accessed on 5 December 2025).
22. StepperOnline. *NEMA 17 Stepper Motor Bipolar Datasheet*. Available online: <https://www.omc-stepperonline.com/download/17HS19-2004S1.pdf> (accessed on 5 December 2025).
23. STMicroelectronics. *L298N Dual H-Bridge Motor Driver Datasheet*. Available online: <https://www.st.com/resource/en/datasheet/l298.pdf> (accessed on 5 December 2025).
24. Generic Electronics Suppliers. *LCD 20x4 Display with I²C Interface Datasheet*. Available online: <https://www.sparkfun.com/datasheets/LCD/HD44780.pdf> (accessed on 5 December 2025).
25. Generic Electronics Suppliers. *Tactile Push Button Switch for Breadboard*. Available online: <https://www.adafruit.com/product/367> (accessed on 5 December 2025).
26. USB Implementers Forum. *USB Type-C Cable Specification*. Available online: <https://www.usb.org/sites/default/files/USB%20Type-C%20Spec%20R2.0%20-%20August%202019.pdf> (accessed on 5 December 2025).
27. IEEE. *IEEE Standard for Wireless LAN Medium Access Control (MAC) and Physical Layer (PHY) Specifications*. Available online: <https://ieeexplore.ieee.org/document/9363693> (accessed on 5 December 2025).
28. Generic Electronics Suppliers. *Dupont Jumper Wires (Male-Female and Female-Female)*. Available online: <https://www.adafruit.com/category/289> (accessed on 5 December 2025).
29. Generic Electronics Suppliers. *Plastic Project Enclosure Box (135x75x40 mm)*. Available online: <https://www.digikey.com/en/products/filter/enclosures/287> (accessed on 5 December 2025).

30. Generic Electronics Suppliers. *AC-DC Power Adapter 12V/1A*. Available online: <https://www.digikey.com/en/products/filter/power-supplies-external-internal-off-board/171> (accessed on 5 December 2025). 440
441
442
31. Insta360. *Insta360 Link—4K AI Webcam Technical Specifications*. Available online: <https://onlinemanual.insta360.com/link/en-us/introduction> (accessed on 5 December 2025). 443
444
32. Raspberry Pi Ltd. *Raspberry Pi 4 Model B Product Brief*. Available online: <https://datasheets.raspberrypi.com/rpi4/raspberry-pi-4-product-brief.pdf> (accessed on 5 December 2025). 445
446
33. EMQ Technologies Co., Ltd. *EMQX—MQTT Platform for IoT Data Streaming Documentation*. Available online: <https://docs.emqx.com/en/emqx/v5.0/> (accessed on 5 December 2025). 447
448
34. EMQ Technologies Co., Ltd. *MQTTX: Your All-in-One MQTT Client Toolbox Documentation*. Available online: <https://mqtx.app/docs> (accessed on 5 December 2025). 449
450
35. OpenJS Foundation. *Node.js API Documentation*. Available online: <https://nodejs.org/api/> (accessed on 5 December 2025). 451
452
36. OpenJS Foundation. *Express API Reference*. Available online: <https://expressjs.com/en/4x/api.html> (accessed on 5 December 2025). 453
454
37. MongoDB, Inc. *MongoDB Documentation*. Available online: <https://www.mongodb.com/docs/manual/> (accessed on 5 December 2025). 455
456
38. Mongoose. *Mongoose ODM API Documentation*. Available online: <https://mongoosejs.com/docs/api.html> (accessed on 5 December 2025). 457
458
39. Vercel, Inc. *Next.js Documentation*. Available online: <https://nextjs.org/docs> (accessed on 5 December 2025). 459
460
40. Meta Platforms, Inc. *React Reference Documentation*. Available online: <https://react.dev/reference/react> (accessed on 5 December 2025). 461
462
41. Arduino AG. *Arduino IDE 2.x Documentation*. Available online: <https://www.arduino.cc/en/software> (accessed on 5 December 2025). 463
464
42. Python Software Foundation. *Python 3 Documentation*. Available online: <https://docs.python.org/3/> (accessed on 5 December 2025). 465
466
43. Eraser Labs, Inc. *Eraser—AI Co-Pilot for Technical Design and Documentation*. Available online: <https://www.eraser.io> (accessed on 5 December 2025). 467
468
44. OpenAI. *ChatGPT*. Available online: <https://chat.openai.com> (accessed on 23 January 2026). Content generated with the assistance of ChatGPT. 469
470
45. Python Software Foundation. *Python 3 Documentation*. Available online: <https://docs.python.org/3/> (accessed on 5 December 2025). 471
472
46. Santiago Sosa Mejía. *RemotePhysicsLab: Prototipo de laboratorio de física híbrido basado en IoT*. Repositorio GitHub. Available online: <https://github.com/waltersosa/RemotePhysicsLab.git> (accessed on 5 December 2025). 473
474
475